NASA Technical Memorandum 86368

Modifications to the Nozzle Test Chamber To Extend Nozzle Static-Test Capability

J. Wayne Keyes

MAY 1985

NASA

NASA Technical Memorandum 86368

Modifications to the Nozzle Test Chamber To Extend Nozzle Static-Test Capability

J. Wayne Keyes
Langley Research Center
Hampton, Virginia

NASA
National Aeronautics
and Space Administration

Scientific and Technical
Information Branch

1985

SUMMARY

The nozzle test chamber at the Langley Research Center has been modified to provide a high-pressure-ratio nozzle static-test capability. Experiments were conducted to determine the range of the ratio of nozzle total pressure to chamber pressure and to make direct nozzle thrust measurements using a three-component strain-gage force balance. Pressure ratios from 3 to 285 have been measured with several axisymmetric nozzles at a nozzle total pressure of 15 to 190 psia. Devices for measuring system mass flow were calibrated using standard axisymmetric convergent choked nozzles. System mass-flow rates up to 10 lbm/sec were measured. In general, the measured thrust results of these nozzles were in good agreement with one-dimensional theoretical predictions for convergent nozzles.

INTRODUCTION

Advanced concepts for Mach 4 to Mach 5 aircraft require turbojet and ramjet power plants with axisymmetric and/or three-dimensional nozzles. These nozzles operate at nozzle pressure ratios approaching 300 during cruise conditions; these pressure ratios are significantly higher than those that can be currently achieved in static test facilities with the nozzle flow exhausting into the atmosphere. Presently, most nozzle testing at the Langley Research Center is conducted in the Langley 16-foot Transonic Tunnel (16'TT) and its nozzle static test stand at free-stream Mach numbers up to 1.3 and nozzle pressure ratios up to 30, depending on nozzle throat area and free-stream Mach number. Therefore, to obtain the experimental data necessary to establish performance standards and validate numerical prediction methods, the nozzle test chamber at the Langley Research Center (ref. 1) has been modified to provide nozzle pressure ratios up to 285 and to measure nozzle thrust directly with a static-test apparatus similar to that used in the 16'TT test stand.

The nozzle test chamber (NTC) consists of a vacuum chamber connected to a 600-psia heated air supply and two vacuum spheres. The exhaust flow of a nozzle mounted inside the chamber discharges into a 60-ft-diameter vacuum sphere through an adjustable flow diffuser, and the test chamber is connected separately to a 41-ft-diameter vacuum sphere. The NTC has been previously used in the Hypersonic Research Engine project (ref. 1), in basic investigations of nozzle flow disturbance levels (ref. 2), and as a pilot facility for the pilot low-disturbance tunnel at the Langley Research Center (ref. 3).

The present paper discusses the modification to the NTC required for the high-pressure-ratio nozzle tests, checkout of the system, and calibration of the mass-flow measuring devices using standard convergent choked nozzles. Thrust measurements obtained on these nozzles using a strain-gage balance are compared with theoretical one-dimensional values determined from the method of reference 4.

SYMBOLS

A	cross-sectional area, in^2
A_{max}	maximum cross-sectional area of calibration nozzle, in^2

a	axial distance from calibration nozzle exit to origin of radius of curvature for inside nozzle contour, in. (fig. 7)
C^*	critical flow factor based on total pressure and temperature upstream of nozzle throat
C_d	discharge coefficient
$C_{F,S}$	stream thrust coefficient
$C_{F,S,I}$	ideal stream thrust coefficient
d	diameter, in.
d_{IS}	inside diameter of instrumentation section, 5.064 in.
$F_{A,ATT}$	balance axial-force attitude tare correction, lbf
$F_{A,BAL}$	total balance axial-force measurement, lbf
$F_{A,BEL}$	balance axial-force bellows tare correction, lbf
$F_{A,BTL}$	balance axial-force correction for boattail pressure effect, lbf
$F_{A,MOM}$	balance axial-force momentum tare correction, lbf
F_I	nozzle ideal thrust for complete expansion of flow, lbf
F_J	measured nozzle thrust, lbf
g	acceleration due to gravity, 32.174 ft/sec^2
I_{CH}	intercept of sonic nozzle discharge coefficient curve
K_{CH}	slope of curve for sonic nozzle discharge coefficient
ℓ	length of sonic nozzle throat, in. (fig. 6)
ℓ_{BTL}	calibration nozzle boattail length, in. (fig. 7)
ℓ_{CN}	total length of calibration nozzle, in. (fig. 7)
M	Mach number
$\dot{m}$	mass-flow rate, lbm/sec
p_{BEL}	static pressure in bellows region of low-pressure plenum chamber, psia
p_{BOX}	static pressure in vacuum chamber, psia
p_{BTL}	average static pressure on boattail section of calibration nozzle, psia
p_{CH}	total pressure in high-pressure plenum chamber, psia
$p_{T,J}$	nozzle total pressure in instrumentation section, psia

p_∞	free-stream static pressure, psia
R_J	gas constant, 53.34 lbf-ft/lbm-°R
$R_{N,CH}$	Reynolds number based on flow conditions in eight sonic nozzles and sonic throat diameter
$R_{N,CN}$	Reynolds number based on sonic flow conditions in calibration nozzle and nozzle throat diameter
r	calibration nozzle internal contour radius, in. (fig. 7)
r_i	radius of sonic nozzle inlet, in. (fig. 6)
r_t	calibration nozzle internal contour radius at nozzle throat, in. (fig. 7)
s	axial distance from calibration nozzle exit to tangency point of nozzle internal contours, in. (fig. 7)
T_{CH}	total temperature in high-pressure plenum chamber, °R
$T_{T,J}$	total temperature in instrumentation section, °R
x	total-pressure-rake tube location measured from wall, in.
x_{DIF}	distance from calibration nozzle exit to entrance plane of adjustable diffuser, in. (fig. 12)
γ	ratio of specific heats

Abbreviations:

diam	diameter
i.d.	inside diameter
NTC	nozzle test chamber at the Langley Research Center
PV	pressure valve
VV	vacuum valve
16'TT	Langley 16-foot Transonic Tunnel
41'SPH	41-ft-diameter vacuum sphere
60'SPH	60-ft-diameter vacuum sphere

Subscripts:

AV	average
a	actual or measured

b	base
CH	high-pressure plenum chamber
CN	calibration nozzle
CP	perforated plate
e	exit
I	ideal
i	inlet
T	total or stagnation
t	throat

APPARATUS AND PROCEDURES

Modifications to NTC Piping

Most of the existing high-pressure piping and vacuum system for the NTC (fig. 1) remained unchanged. Modifications were made to the high-pressure piping upstream of the test chamber (fig. 2(a)) and included new piping, flexible hoses, and manifolds to supply air to the static-test apparatus installed in the NTC. The NTC static-test apparatus was patterned after the apparatus used for low-nozzle-pressure ratio testing in the Langley 16-foot Transonic Tunnel (ref. 5) and in the 16'TT static-test stand exhausted to atmosphere (ref. 6). The upstream half of the NTC settling chamber (ref. 3) was retained as an air filter, because it contained filter paper, several porous metal plates, and wire-mesh screens. A new end plate and strut were fabricated to support the NTC apparatus in the vacuum chamber. (See fig. 2.) The centerline of the NTC test apparatus was located along the centerline of the NTC and positioned such that the nozzle exhaust flow could be observed in the schlieren window (fig. 2(c)). Typical schlieren photographs of a calibration nozzle exhaust flow are shown in figure 3.

Test Procedure

The basic NTC mode of operation was not altered for these tests. Nozzle total pressure $p_{T,J}$ was controlled using pressure valves PV3 and/or PV4, depending on the nozzle mass-flow required; nozzle total temperature $T_{T,J}$ was controlled using pressure valves PV1 and PV2. (See fig. 1.) The nozzle model exhaust passes through the adjustable diffuser and through vacuum VV1 to the 60-ft-diameter sphere (60'SPH) or through VV6 to atmosphere. Test-chamber vacuum level can be regulated by using vacuum valves VV3, VV4, and VV5 to the 41-ft-diameter sphere (41'SPH) or VV2 to the 60'SPH. For example, to obtain high ratios of nozzle total pressure to test chamber pressure ($285 > p_{T,J}/p_{BOX} > 125$), VV1 would be 100 percent open, VV2 and VV6 closed, and VV3, VV4, and VV5 open. Test-chamber pressure can be increased ($p_{T,J}/p_{BOX}$ decreased) by systematically closing VV5 and/or VV4 and throttling VV3. Moderate ratios ($150 > p_{T,J}/p_{BOX} > 50$) can be obtained by closing VV3, VV4, and VV5 and throttling both VV2 and VV1 within certain limits. Low values of $p_{T,J}/p_{BOX}$ result

when both the nozzle flow and test chamber are exhausted to atmosphere or when the 41'SPH vacuum level is increased and p_{BOX} is varied by throttling VV3 with VV2, VV4, and VV5 closed.

Test Conditions

The nozzle total pressure $p_{T,J}$ is limited to 190 psia by the stainless-steel bellows of the test apparatus shown in figure 4. Nozzle total pressure can be further limited by the sonic nozzle throat area, the thrust balance capacity, and/or the model pressure instrumentation, to a maximum of 115 psia. (See fig. 5.) The nozzle total temperature is normally ambient (540°R) with a maximum limit of 660°R. Vacuum-chamber pressure varies from approximately 0.2 to 14 psia.

Test Apparatus and Instrumentation

Figure 4(b) is a schematic of the NTC apparatus. Six high-pressure hoses (0.562-in. i.d.) supply air to the annular high-pressure plenum chamber of the sting. The high-pressure plenum chamber was instrumented to measure pressure and temperature (p_{CH} and T_{CH}, respectively). The airflow, indicated by arrows, was introduced perpendicular to the sting axis through eight multithroat sonic nozzles (fig. 6), which were equally spaced around the center core to minimize any air momentum effects on axial force. Two sets of sonic nozzles were used. Each sonic nozzle of the first set (fig. 6(a)) consisted of seven 0.113-in-diameter throats, each approximately 5.3 diameters long with a 0.04-in. entrance radius, for a total flow area $A_{t,CH,T}$ of 0.562 in^2. The second set of nozzles (fig. 6(b)) had a total flow area of 1.070 in^2, and each nozzle consisted of seven 0.156-in-diameter throats approximately 3.8 diameters long with a sharp corner entrance. The eight radial sonic nozzles, which serve as the minimum flow area of the total system, were mounted in a ring attached to the nonmetric sting; therefore, the balance measures thrust due to the acceleration of the air through the metric nozzle. Two metal bellows, silver-soldered on either side of the sonic nozzle ring, served as flexible seals between the metric low-pressure plenum and the nonmetric sting.

The metric part of the test apparatus (low-pressure plenum, instrumentation section, and nozzle) was supported by the balance and is indicated by cross-hatching in figure 4(b). Interchangeable three-component balances can be used, depending on the total throat area of the eight sonic nozzles and the throat area of the model nozzle. The balance is covered by a fairing to streamline the flow from the low-pressure plenum chamber to the instrumentation section. Either a pair of screens fabricated from 0.25-in. mesh, 0.026-in-diameter wire cloth and backed by four 0.05-in-thick sharp support vanes, or a perforated plate was used as a flow straightener. The instrumentation section contained a five-tube (0.040-in. i.d. tubing) pressure rake to measure $p_{T,J}$ and a shielded thermocouple probe (36-gage iron constantan wire) to measure $T_{T,J}$. Various axisymmetric calibration nozzles were attached at a sealed joint downstream of the instrumentation section. Additional instrumentation sections for square and rectangular nozzles are shown in figure 4(a). External static pressures were measured near the exit of the calibration nozzle to check for boattail pressure effects on balance axial force.

Calibration Nozzles

Standard axisymmetric convergent nozzles (ref. 6) were used to calibrate the mass-flow rate through the NTC apparatus; these choked nozzles are of the type described in references 7 and 8. Five 16'TT nozzles which matched the specifications of reference 8 ($r_t/d_t > 2$), with nominal throat areas $A_{t,CN}$ of 1.000, 1.932, 3.000, 3.999, and 5.731 in^2, respectively, were used. A sketch of a typical 16'TT nozzle is shown in figure 7(a). Additional NTC calibration nozzles with a different mounting were made but not tested in the current study. (See fig. 7(b).) Calibration nozzles 16'TT-2 ($A_{t,CN}$ = 1.932 in^2) and 16'TT-5 ($A_{t,CN}$ = 5.731 in^2) were calibrated using several primary standard nozzles at the Colorado Engineering Experimental Station of the University of Colorado, and the calibration curves for these two nozzles from unpublished data of Wood and Runckel are presented in figure 8. In general, the calibration-curve data in figure 8 agree with theoretical values of reference 7. Primary standard nozzles have known discharge coefficients, which have been verified by laboratories such as the National Bureau of Standards. (See ref. 9.)

DATA REDUCTION

Force, pressure, and temperature data were recorded and stored on a multichannel recording system at a sampling rate of 20 frames per second. Each data point consisted of 200 frames of data averaged over 10 seconds. A desk-top computer was used to compute on-line data while making a test run.

Mass-Flow and Ideal-Thrust Calculations

The measured mass flow for any given model nozzle is

$$\dot{m}_a = (C_{d,CH})\left(\frac{p_{CH}}{\sqrt{T_{CH}}}\right)(A_{t,CH,T})C^*_{CH}\sqrt{\frac{g}{R_J}} \tag{1}$$

which is the actual mass flow through the eight sonic nozzles. The critical flow factor C^*_{CH}, which is defined in reference 10, is a function of plenum pressure and temperature and accounts for any real-gas or compressibility effects in the sonic throat. (See refs. 9 and 10.) The calibration of these sonic nozzles is discussed in the "Results and Discussion" section.

The basic nozzle static performance parameter is the ratio of the measured nozzle thrust to the ideal thrust F_J/F_I for complete expansion of the nozzle flow to ambient conditions. The ideal thrust is defined (from ref. 4) by

$$F_I = \dot{m}_a\sqrt{\frac{2\gamma}{\gamma - 1}\left(\frac{R_J}{g}\right)(T_{T,J})\left[1 - \left(\frac{p_{BOX}}{p_{T,J}}\right)^{\left(\frac{\gamma-1}{\gamma}\right)}\right]} \tag{2}$$

Measured Thrust and Static Performance

The measured nozzle thrust F_J is obtained from the total balance axial-force measurement, which has been corrected for weight tares and the usual balance interactions, and is defined as

$$F_{A,BAL} = F_J + F_{A,BEL} + F_{A,MOM} + F_{A,ATT} + F_{A,BTL} \tag{3}$$

or

$$F_J = F_{A,BAL} - (F_{A,BEL} + F_{A,MOM} + F_{A,ATT} + F_{A,BTL}) \tag{4}$$

where $F_{A,ATT} = 0$ (angle of attack of model nozzle equals zero) and the axial-force correction for jet effects on the calibration nozzle boattail is

$$F_{A,BTL} = (p_{BTL,AV} - p_{BOX})(A_{max} - A_{t,CN}) \tag{5}$$

The bellows tare correction $F_{A,BEL}$ and the momentum tare correction $F_{A,MOM}$ were determined by running the calibration nozzles with known performance over a range of combined balance loads as discussed in references 6 and 11. These tares result from a small pressure difference between the ends of the bellows caused by high internal velocities and from small differences in the two bellows spring constants when the bellows are pressurized (ref. 6). The measured axial-force data were corrected in a manner similar to that discussed in reference 11. Similar corrections can be applied to the normal-force and pitching-moment data.

Stream thrust coefficient (or impulse function) is a function of measured total thrust adjusted by the free-stream pressure-area term, nozzle total pressure, and throat area, and is defined as

$$C_{F,S} = \frac{F_J + p_\infty A_e}{p_{T,J}(A_{t,CN})} \tag{6}$$

For the calibration nozzles of the present test, $A_e = A_{t,CN}$ and $p_\infty = p_{BOX}$. The ideal value, which is a function of local Mach number, is

$$C_{F,S,I} = \frac{1 + \gamma M_e^2}{\left[1 + \left(\frac{\gamma - 1}{2}\right) M_e^2\right]^{\left(\frac{\gamma}{\gamma-1}\right)}} \tag{7}$$

RESULTS AND DISCUSSION

Calibration of System Mass Flow Rate

The eight radial multithroat sonic nozzles (fig. 6) located between the low-pressure and high-pressure plenums were used to measure the mass-flow rate of the total system. An effective discharge coefficient ($C_{d,CH}$) for the eight sonic nozzles, which constitutes the minimum flow area of the system, was calculated using the actual mass flow through the calibration nozzle. The actual mass-flow rate through the calibration nozzle is

$$\dot{m}_{a,CN} = C_{d,CN}(\dot{m}_{I,CN}) = C_{d,CN}(A_{t,CN}) \frac{p_{T,J}}{\sqrt{T_{T,J}}} \left(C^* \sqrt{\frac{g}{R_J}} \right) \tag{8}$$

where C^* is the critical flow factor and is a function of $p_{T,J}$ and $T_{T,J}$. The calibration nozzle discharge coefficient $C_{d,CN}$ for nozzles 16'TT-1, 16'TT-3, and 16'TT-4 was assumed to be 0.995, based on the predicted level of reference 7; for nozzles 16'TT-2 and 16'TT-5, the actual values from the data fairing of figure 8 were used.

From continuity relations, the actual mass-flow rate through the eight sonic nozzles is equal to the actual flow rate through the calibration nozzle; therefore, the effective discharge coefficient for the sonic nozzles is

$$C_{d,CH} = (\dot{m}_{a,CN}) \frac{\sqrt{\frac{R_J(T_{CH})}{g}}}{p_{CH}(A_{t,CH,T})C^*_{CH}} \tag{9}$$

where the critical flow factor C^*_{CH} is a function of p_{CH} and T_{CH}, and $A_{t,CH,T}$ is the total geometric throat area of the eight sonic nozzles. Figure 9 presents the variation of $C_{d,CH}$ as a function of Reynolds number based on sonic conditions at the throat (see ref. 9) and the geometric diameter of one throat $d_{t,CH}$ for both sets of sonic nozzles. A first-order expression for the data is

$$C_{d,CH} = I_{CH} + K_{CH}(R_{N,CH}) \tag{10}$$

The measured pressure ratios p_{BEL}/p_{CH} presented in figure 10 fall below the theoretical pressure ratio for choked flow; therefore, the eight sonic nozzles are choked for the range of chamber pressures tested, except for the combination of calibration nozzle 16'TT-1 and the set of large sonic nozzles. (See fig. 10(b).) This result would be expected, since the calibration nozzle throat becomes the minimum area for this case ($A_{t,CN} < A_{t,CH,T}$).

Pressure Measurements

The maximum and minimum nozzle pressure ratios obtained are a function of nozzle throat area, box pressure, and nozzle total pressure, and are limited by the force balance used and other structural restraints. For example, pressure ratios from 3 to 285 at $p_{T,J}$ = 15 and 190 psia, respectively, were measured using nozzle 16'TT-1 ($A_{t,CN}$ = 1.000 in^2). Pressure ratios for calibration nozzle 16'TT-4 ($A_{t,CN}$ = 3.999 in^2) were 3 to 50 at the same $p_{T,J}$ values. Mass-flow rates up to 10 lbm/sec were measured in the system.

Typical nozzle total-pressure measurements obtained with the five-tube rake in the instrumentation section with screens are shown in figure 11. The nozzle total-pressure values are normalized by the bellows static pressure upstream of the instrumentation section. In general, for a given nozzle total pressure and a particular calibration nozzle, the variation of the rake pressure measurement is small. This small variation indicates that the Mach number outside the boundary layer is nearly constant across the instrumentation section.

External static pressures were measured on the aft section of the calibration nozzle to determine the jet interference pressure effects in the boattail region. Ratios of the average boattail pressure to box pressure $(p_{BTL}/p_{BOX})_{AV}$ as a function of nozzle pressure ratio are presented in figure 12 for calibration nozzle 16'TT-1. These results indicate that some jet interference effects (0.1 to 0.2 percent of measured thrust) are present at the higher nozzle pressure ratio when the NTC is open to both vacuum spheres. This could be expected, since at the lower box pressures (large nozzle pressure ratios), the jet plume becomes larger, and therefore influences the boattail pressure distribution. The jet interference effect is also a function of the position of the diffuser relative to the nozzle exit.

Static Performance

In general, the variation of nozzle thrust ratio F_J/F_I with nozzle pressure ratio for the five calibration nozzles shows excellent agreement with the theoretical one-dimensional values obtained from expressions of reference 4. (See fig. 13.) The theoretical expression for this curve is a function of the ratio of specific heats and pressure ratio. It is interesting to note the large nozzle underexpansion loss (which was expected) resulting from using a convergent nozzle to generate thrust at high pressure ratios.

Static thrust expressed in terms of stream thrust coefficient is presented in figure 14. The values are constant, as would be expected for choked flow for the range of nozzle pressure ratios tested. The values are slightly lower than the theoretical value of 1.268 (for a local Mach number of 1 from ref. 12), except for the larger-calibration nozzle values, which are higher.

CONCLUDING REMARKS

The modified nozzle test chamber at the Langley Research Center is operational and calibration tests have been completed to determine its operating characteristics. Nozzle pressure ratios from 3 to 285 have been obtained with a 1.000-in^2-throat calibration nozzle at nozzle total pressures from 15 to 190 psia. Pressure ratios from 3 to 50 were measured with a 3.999-in^2 throat nozzle over the same range of nozzle

total pressures. Mass-flow rates up to 10 lbm/sec were measured. Thrust measurements have been made on several axisymmetric convergent calibration nozzles and are in good agreement with theoretical one-dimensional predictions obtained using the method of Runckel and Swihart.

NASA Langley Research Center
Hampton, VA 23665
February 27, 1985

REFERENCES

1. Molloy, John K.; Mackley, Ernest A.; and Keyes, J. Wayne: Effect of Diffusers, Shrouds, and Mass Injection on the Starting and Operating Characteristics of a Mach 5 Free-Jet Tunnel. NASA TN D-6377, 1971.

2. Stainback, P. C.; and Wagner, R. D.: A Comparison of Disturbance Levels Measured in Hypersonic Tunnels Using a Hot-Wire Anemometer and a Pitot Pressure Probe. AIAA Paper No. 72-1003, Sept. 1972.

3. Creel, Theodore R., Jr.; Keyes, J. Wayne; and Beckwith, Ivan E.: Noise Reduction in a Mach 5 Wind Tunnel With a Rectangular Rod-Wall Sound Shield. NASA TP-1672, 1980.

4. Runckel, Jack F.; and Swihart, John M.: A Hydrogen Peroxide Turbojet-Engine Simulator for Wind-Tunnel Powered-Model Investigations. NACA RM L57H15, 1957.

5. Compton, William B., III; and Runckel, Jack F.: Jet Effects on the Boattail Axial Force of Conical Afterbodies at Subsonic and Transonic Speeds. NASA TM X-1960, 1970.

6. Berrier, Bobby L.; and Re, Richard J.: Effect of Several Geometric Parameters on the Static Internal Performance of Three Nonaxisymmetric Nozzle Concepts. NASA TP-1468, 1979.

7. Stratford, B. S.: The Calculation of the Discharge Coefficient of Profiled Choked Nozzles and the Optimum Profile for Absolute Air Flow Measurement. J. R. Aeronaut. Soc., vol. 68, no. 640, Apr. 1964, pp. 237-245.

8. Sparkes, D. W.: A Standard Choked Nozzle for Absolute Calibration of Air Flowmeters. Aeronaut. J., vol. 72, no. 688, Apr. 1968, pp. 335-338.

9. Arnberg, B. T.: Review of Critical Flowmeters for Gas Flow Measurements. Trans. ASME, Ser. D: J. Basic Eng., vol. 84, no. 4, Dec. 1962, pp. 447-460.

10. Johnson, Robert C.: Real-Gas Effects in Critical-Flow-Through Nozzles and Tabulated Thermodynamic Properties. NASA TN D-2565, 1965.

11. Capone, Francis J.: Static Performance of Five Twin-Engine Nonaxisymmetric Nozzles With Vectoring and Reversing Capability. NASA TP-1224, 1978.

12. Tables of Compressible Flow Functions. Pratt & Whitney Aircraft, c.1963.

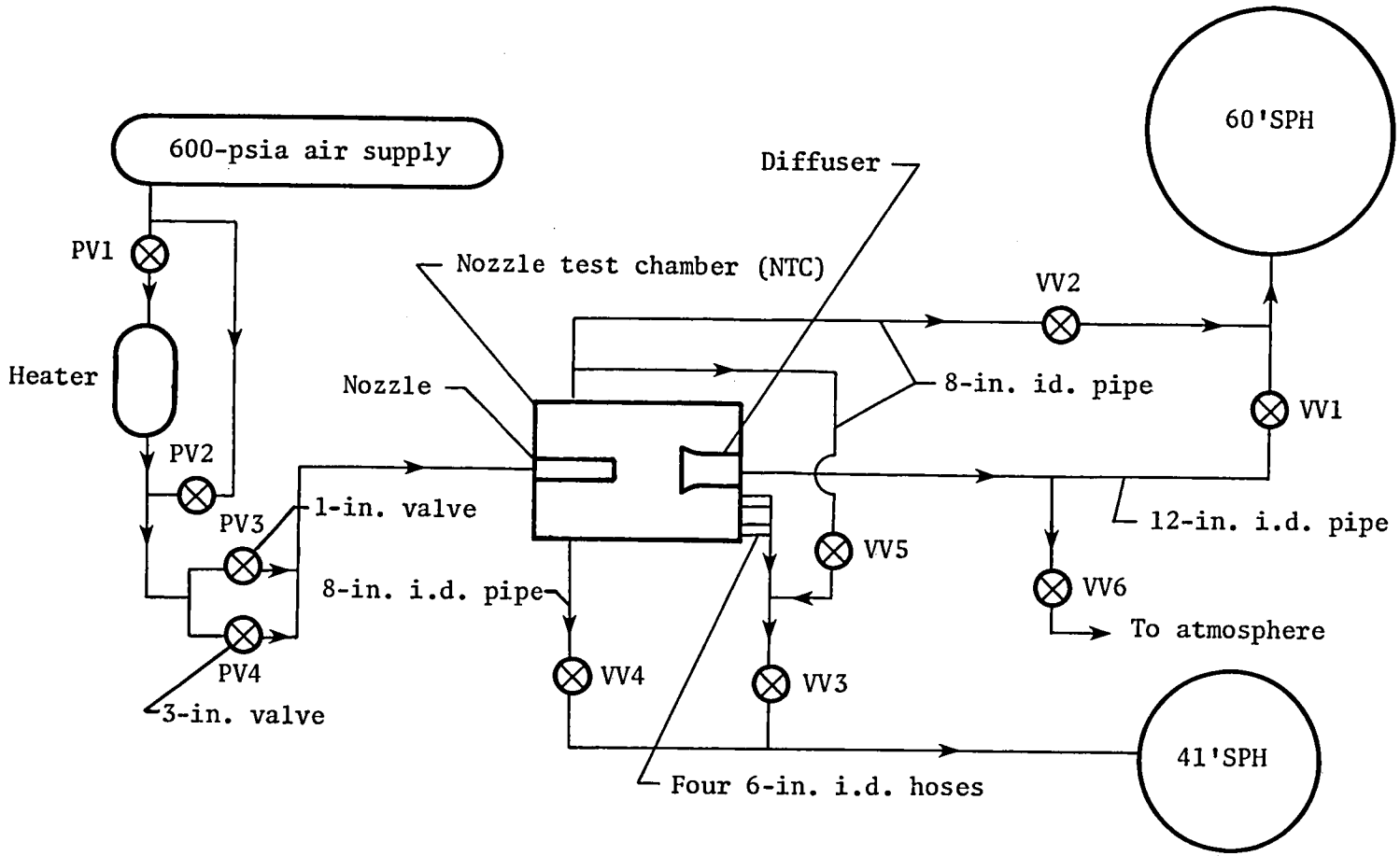

Figure 1.- Schematic of high-pressure piping and vacuum system for nozzle test chamber.

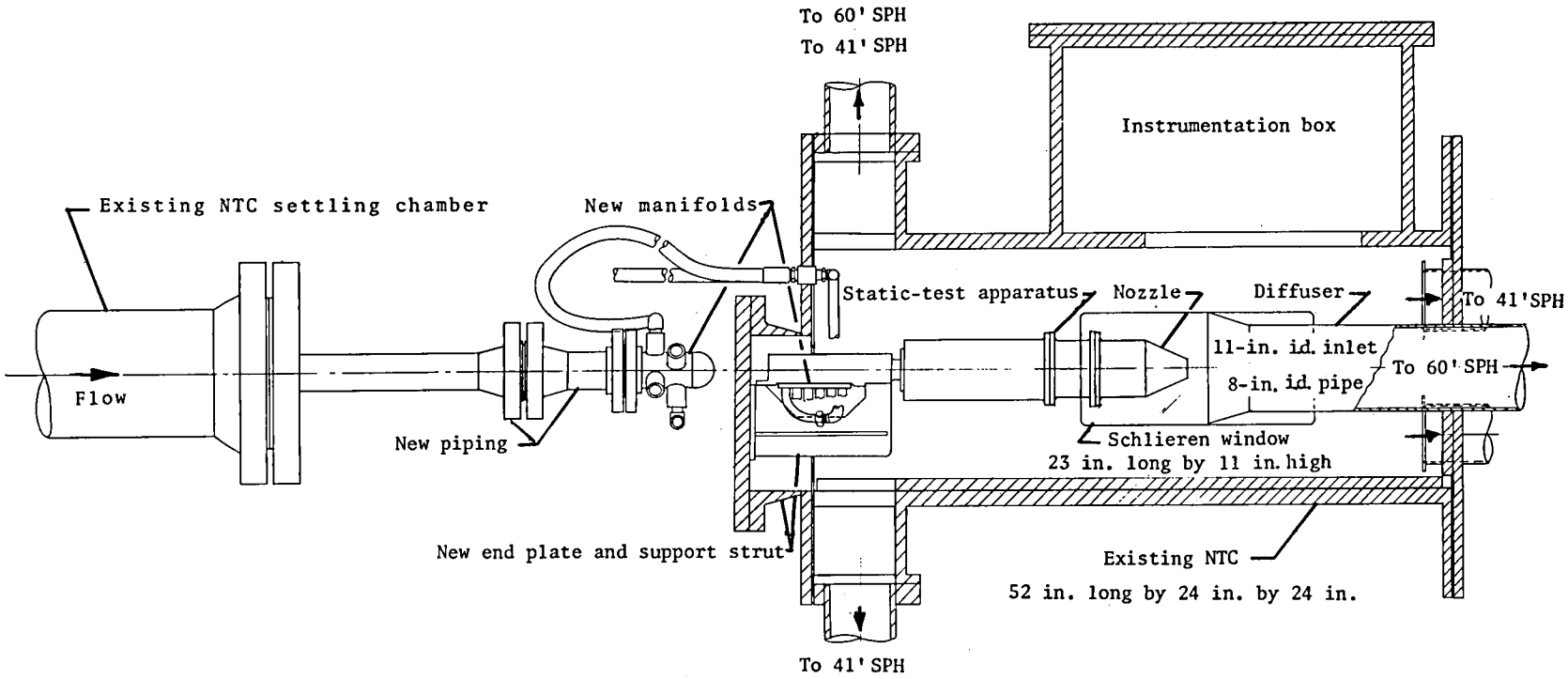

(a) Sketch of nozzle test chamber.

Figure 2.- Modifications to nozzle test chamber.

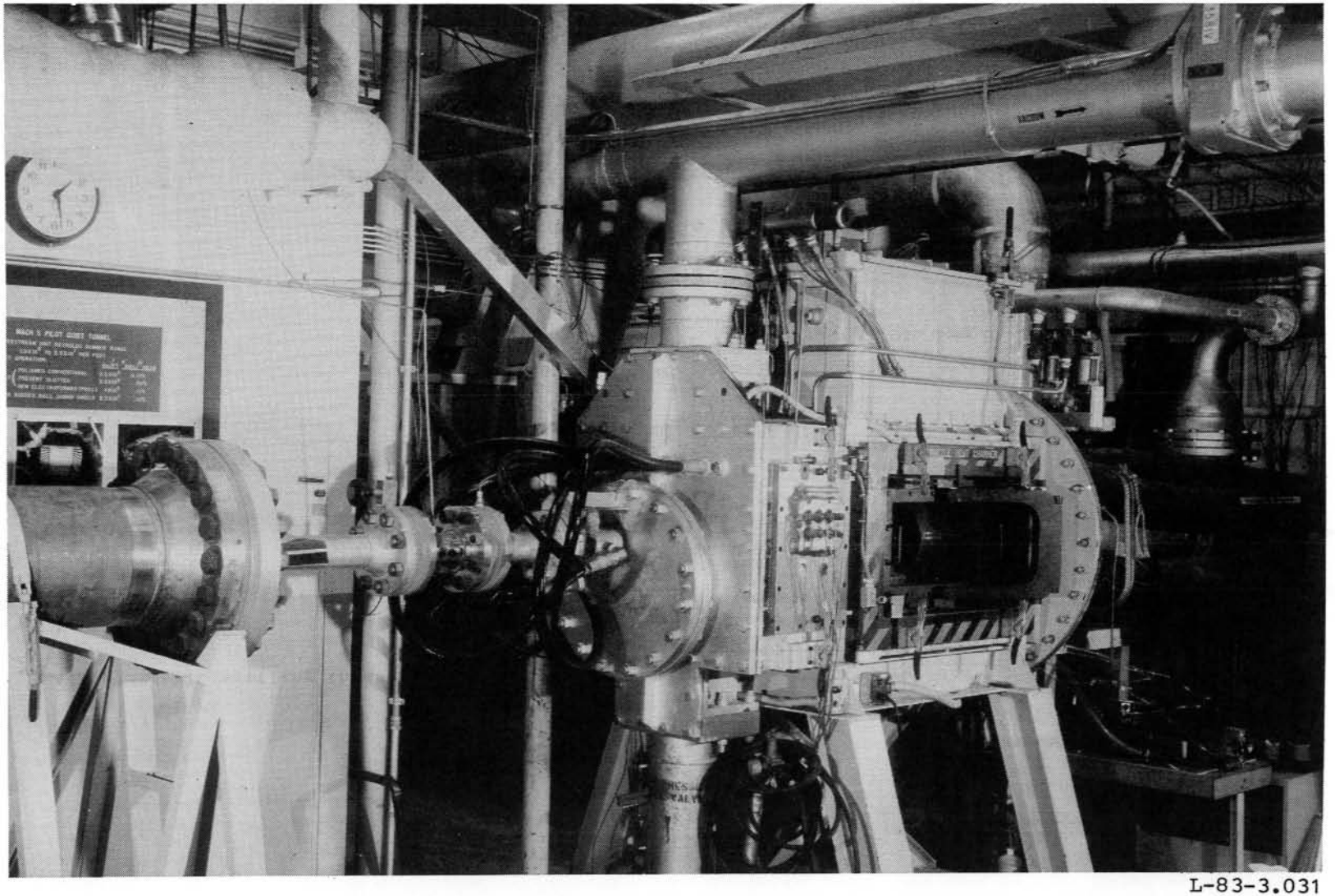

L-83-3.031

(b) Photograph of nozzle test chamber.

Figure 2.- Continued.

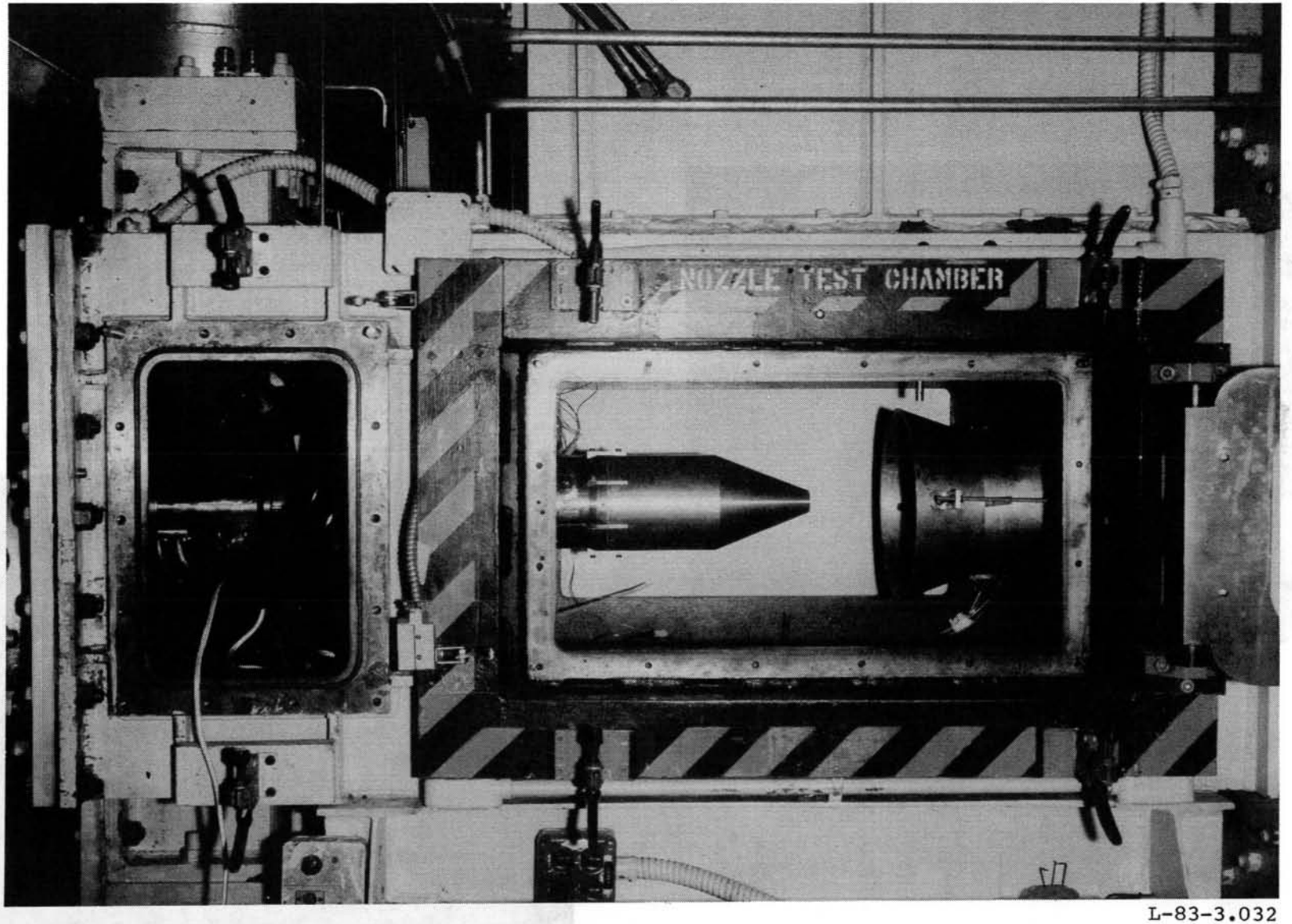

L-83-3.032

(c) Test apparatus mounted in nozzle test chamber.

Figure 2.- Concluded.

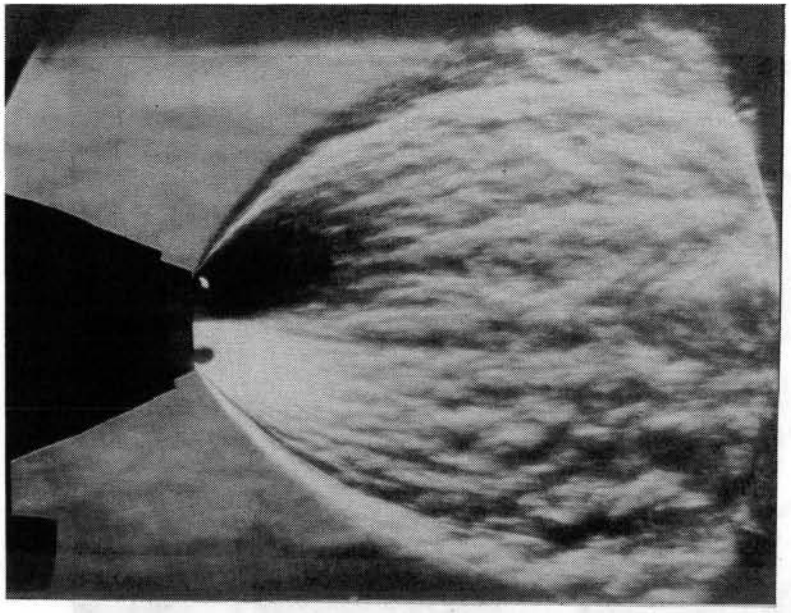

$P_{T,J}/P_{BOX} = 119$

$P_{T,J}/P_{BOX} = 56$

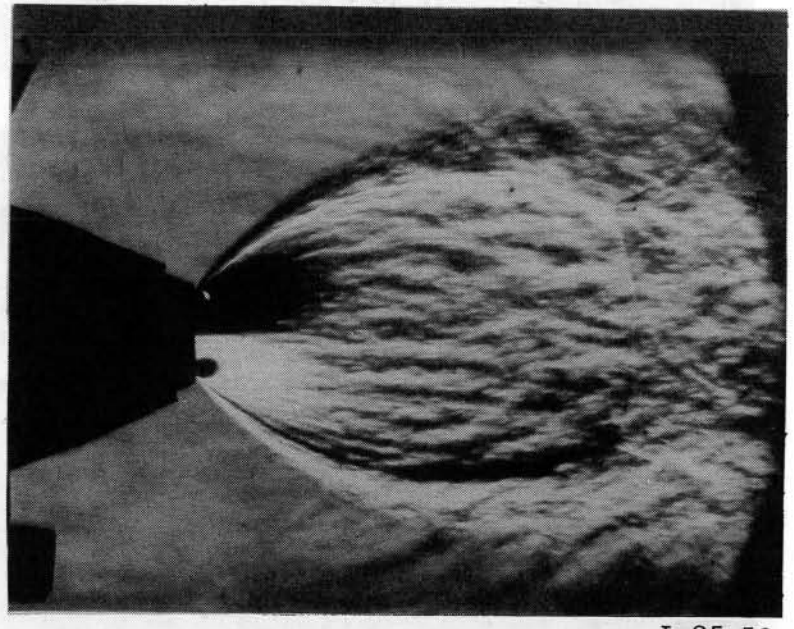

L-85-53

Figure 3.- Typical schlieren photographs of calibration nozzle flow in NTC.

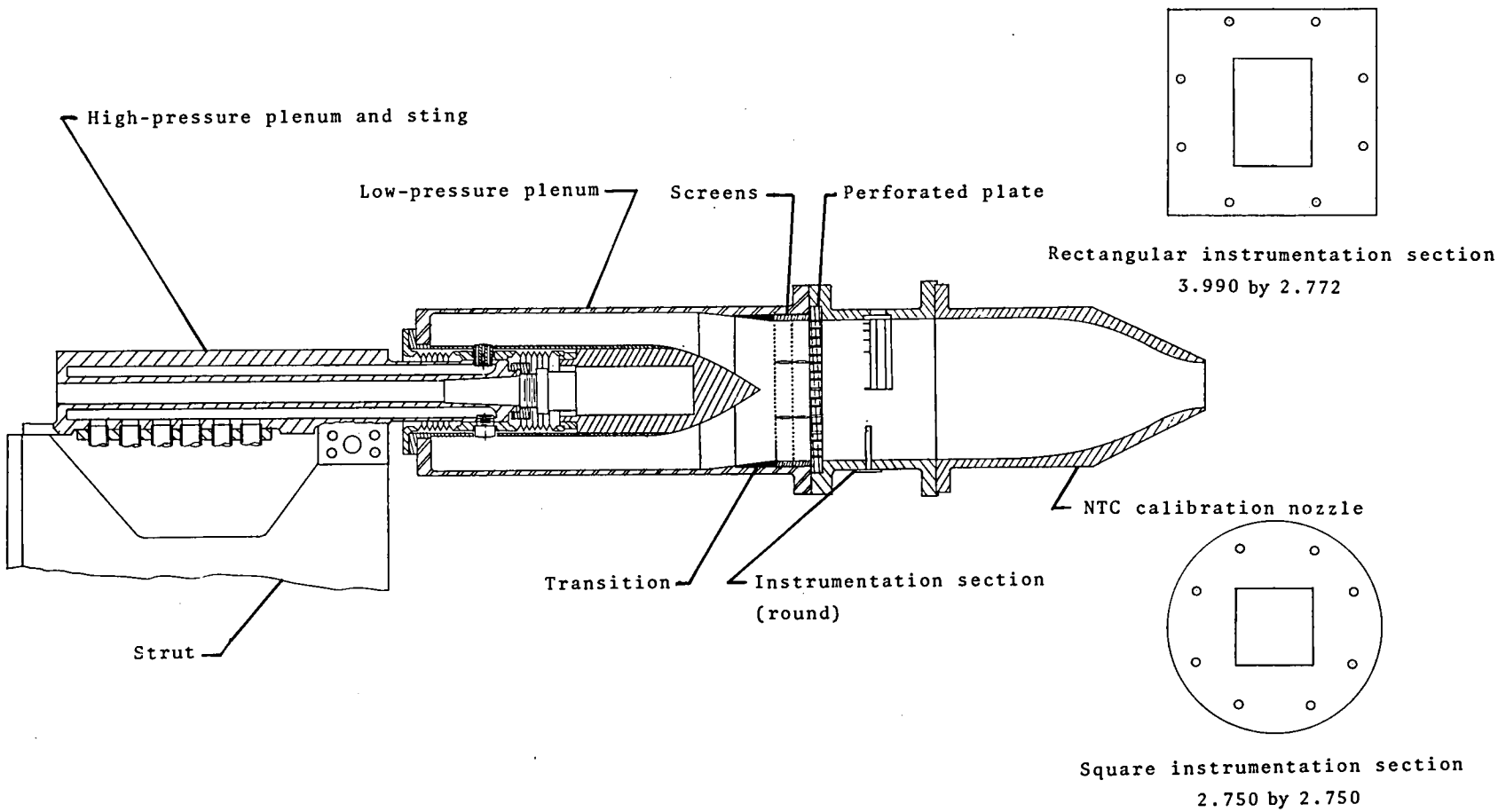

(a) Static-test apparatus with calibration nozzle installed.

Figure 4.- Details of test apparatus and systems. All dimensions in inches.

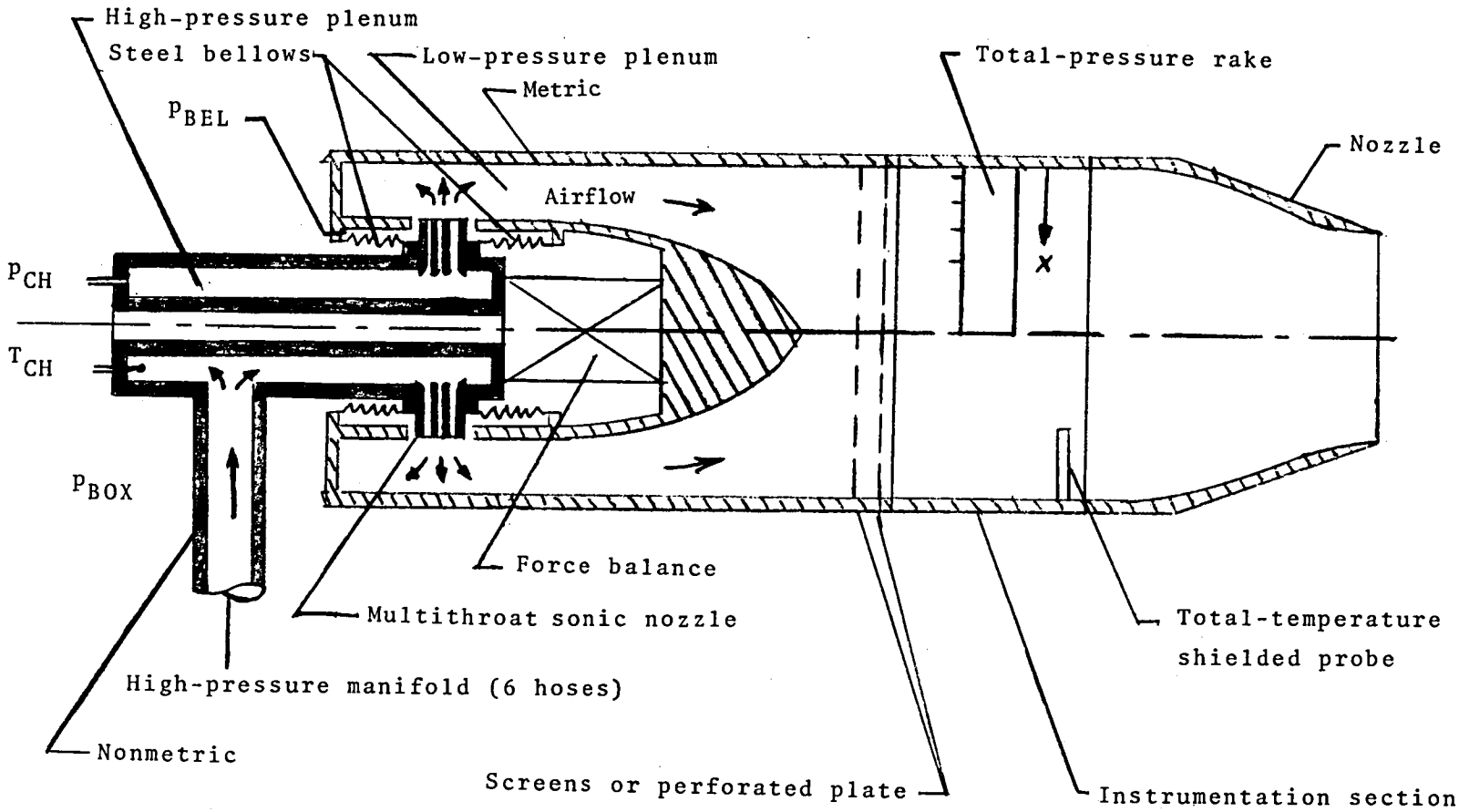

(b) Schematic of nozzle air system and force measuring system.

Figure 4.- Concluded.

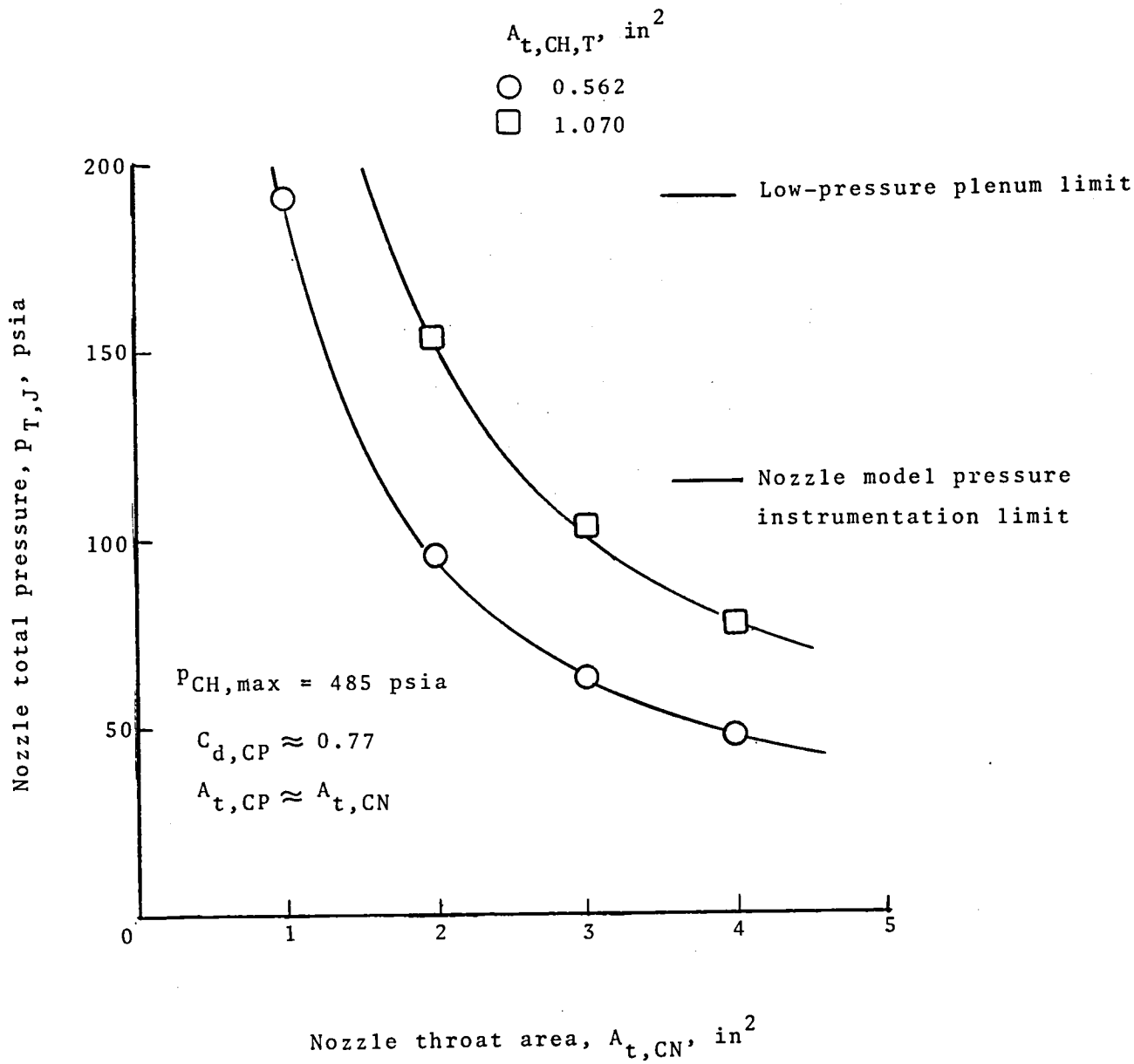

Figure 5.- Variation of maximum nozzle total pressure with model nozzle throat area and sonic nozzle throat area.

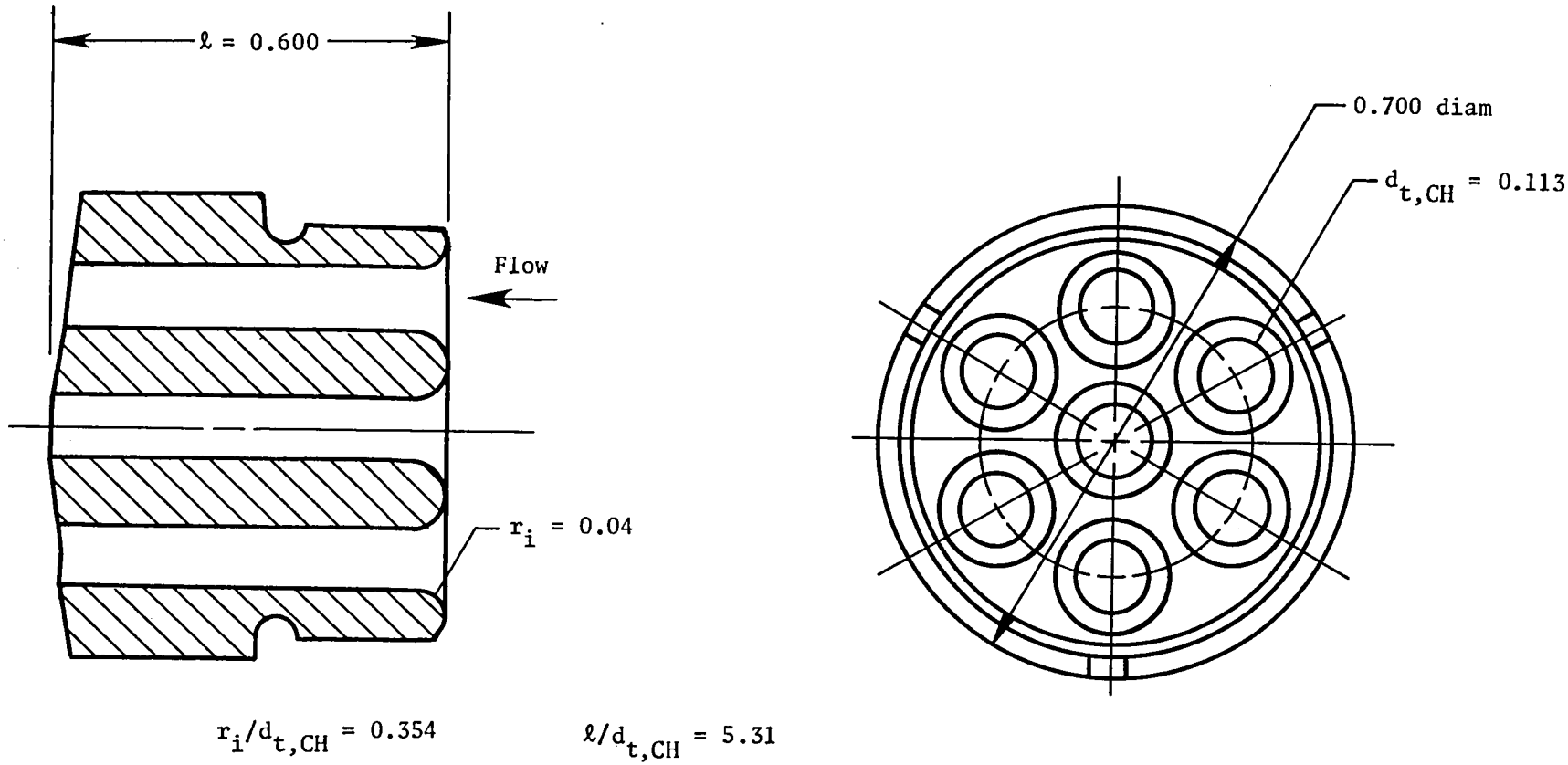

$r_i/d_{t,CH} = 0.354$ $\quad$ $\ell/d_{t,CH} = 5.31$

(a) $A_{t,CH,T} = 0.562$.

Figure 6.- Multithroat sonic nozzles. All dimensions in inches.

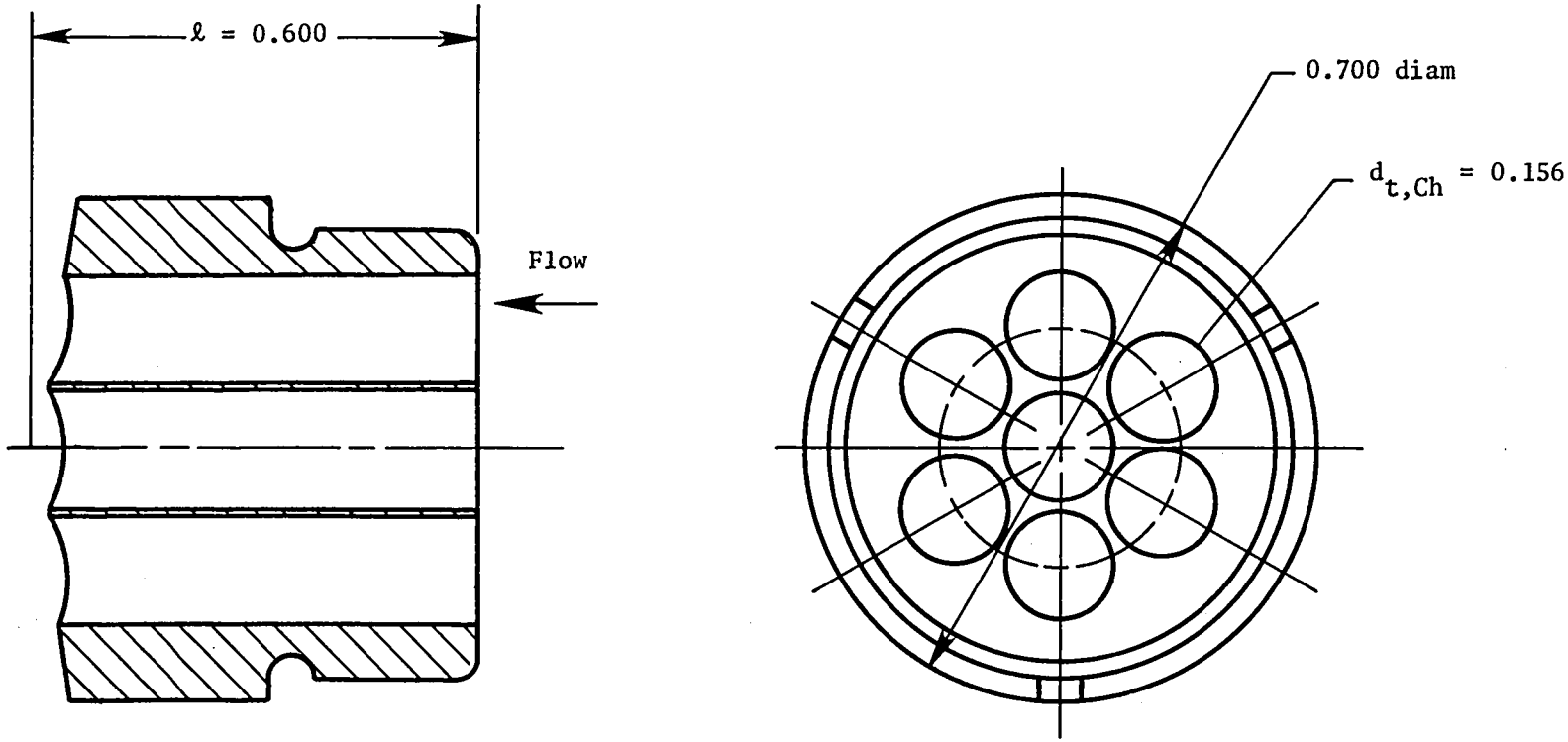

$r_i/d_{t,CH}$ = 0 $\quad$ $\ell/d_{t,CH}$ = 3.85

(b) $A_{t,CH,T}$ = 1.070.

Figure 6.- Concluded.

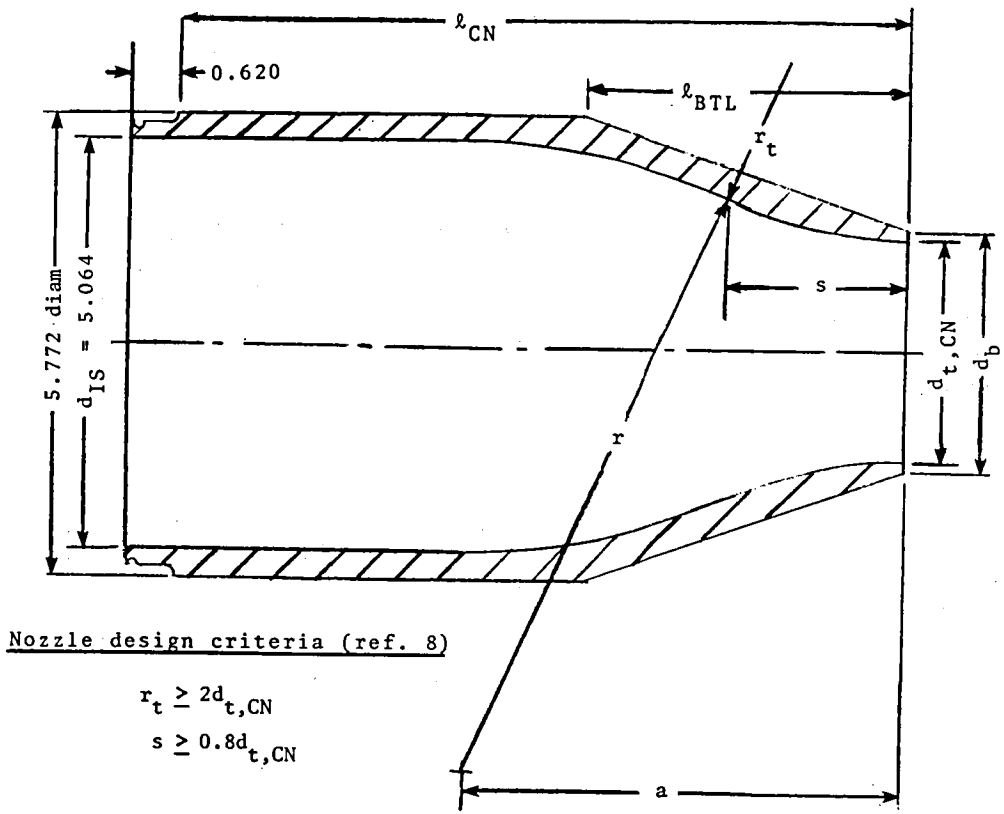

	Nozzle number				
	16'TT-1	16'TT-2	16'TT-3	16'TT-4	16'TT-5
$A_{t,CN}$	.999	1.933	3.002	3.992	5.711
a	9.428	6.274	7.450	5.837	5.432
d_b	1.378	1.820	2.204	2.505	2.950
$d_{t,CN}$	1.128	1.569	1.955	2.255	2.700
ℓ_{BTL}	5.500	4.000	5.000	4.000	4.000
ℓ_{CN}	11.880	9.000	9.000	9.000	9.000
r	21.314	9.000	14.715	8.320	7.700
r_t	2.257	3.140	3.909	4.510	5.400
s	.903	1.623	1.564	2.052	2.239

(a) 16'TT calibration nozzle.

Figure 7.- Sketch of calibration nozzle. All dimensions in inches.

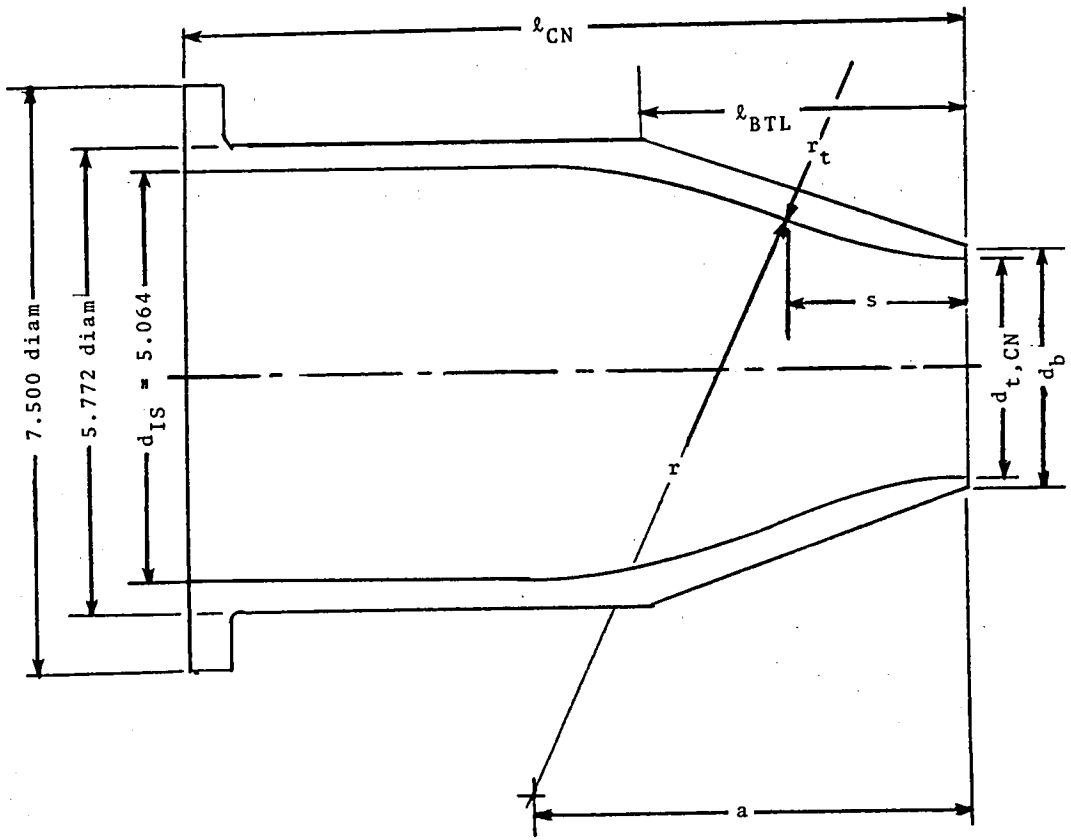

	Nozzle number			
	NTC-1	NTC-2	NTC-3	NTC-4
$A_{t,CN}$	1.010	2.000	3.000	4.000
a	9.431	8.312	7.452	6.725
d_b	1.377	1.856	2.205	2.509
$d_{t,CN}$	1.134	1.596	1.954	2.257
ℓ_{BTL}	5.000	5.000	4.500	4.500
ℓ_{CN}	12.500	11.000	10.000	9.250
r	21.314	17.580	14.714	12.299
r_t	2.257	3.192	3.909	4.514
s	0.903	1.277	1.564	1.805

(b) NTC calibration nozzle.

Figure 7.- Concluded.

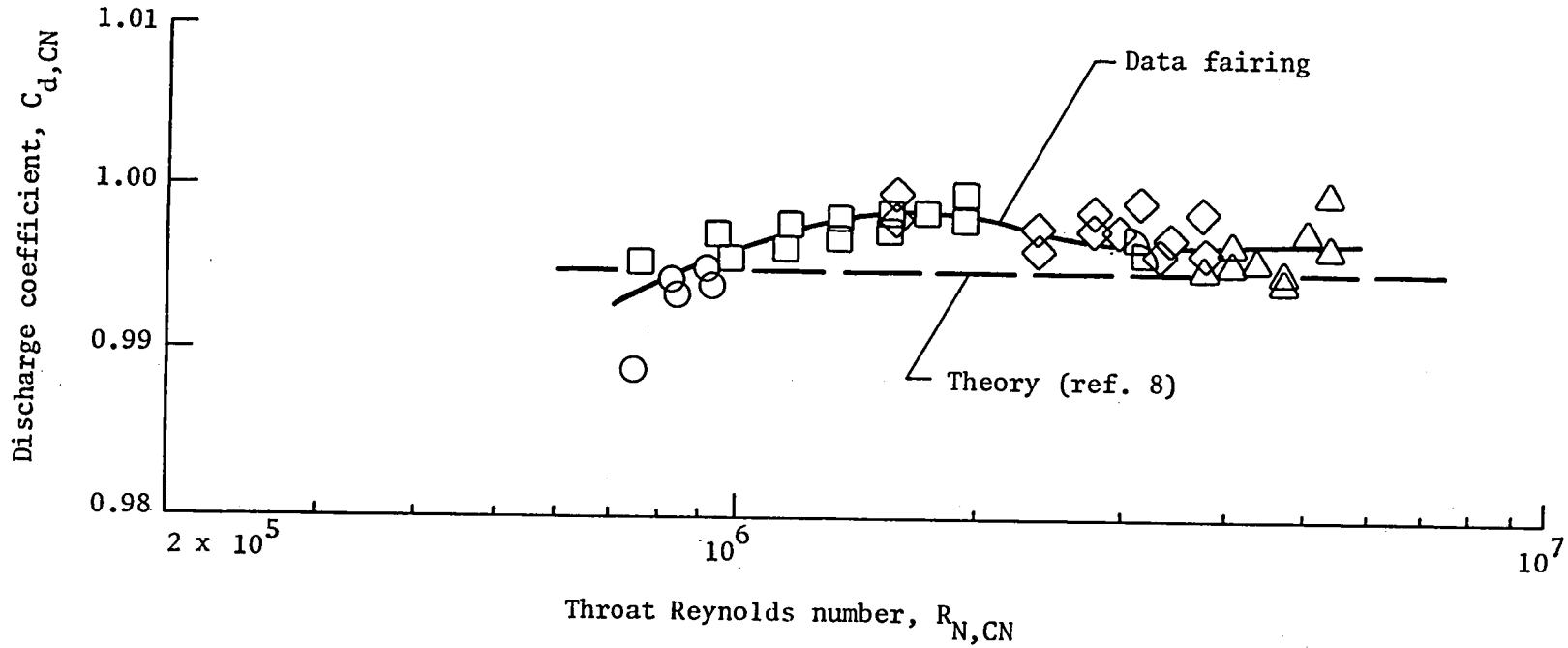

(a) Calibration nozzle 16'TT-2 ($A_{t,CN}$ = 1.932 in^2).

Figure 8.- Calibration of 16'TT calibration nozzles. Unpublished data obtained at The Engineering Experiment Station, University of Colorado.

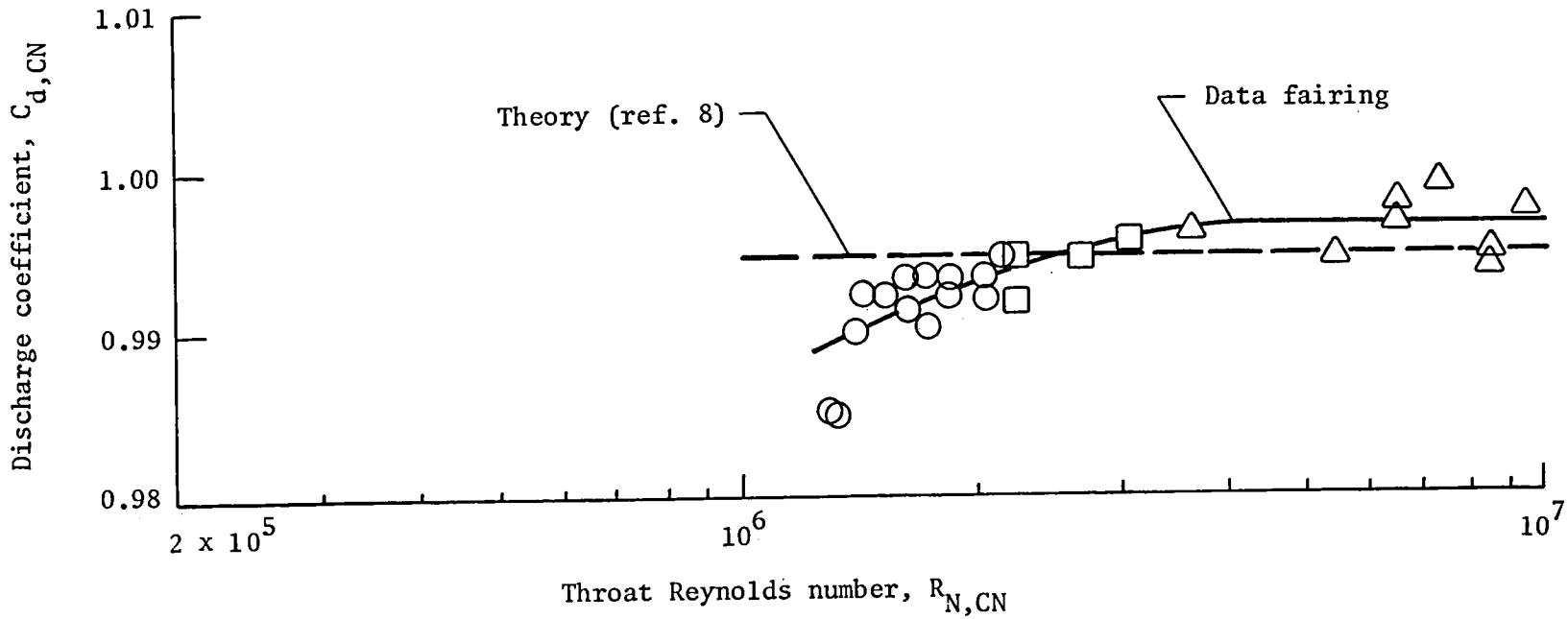

(b) Calibration nozzle 16'TT-5 ($A_{t,CN}$ = 5.731 in^2).

Figure 8.- Concluded.

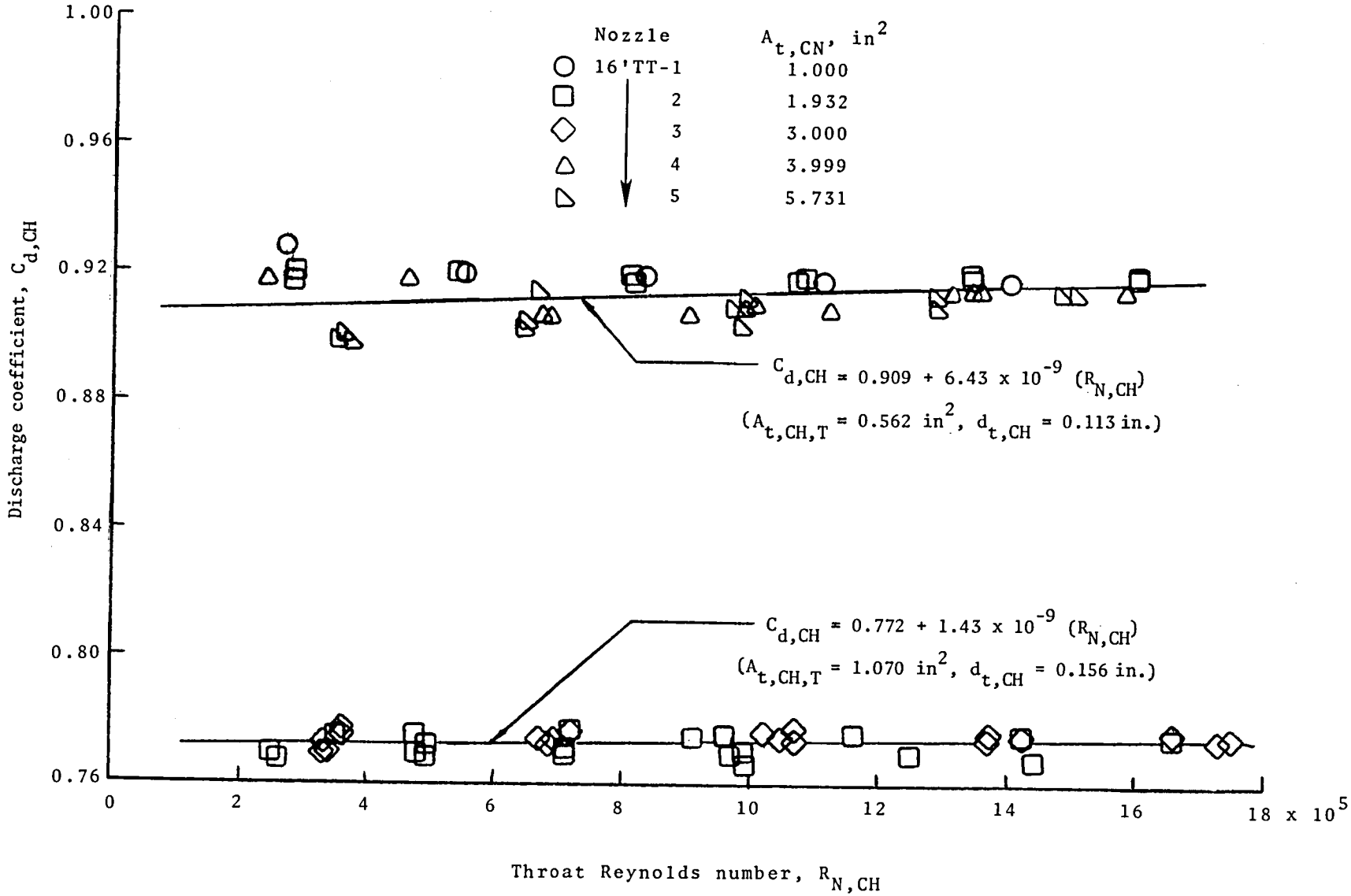

Figure 9.- Discharge coefficient for multithroat sonic nozzles as a function of sonic throat Reynolds number.

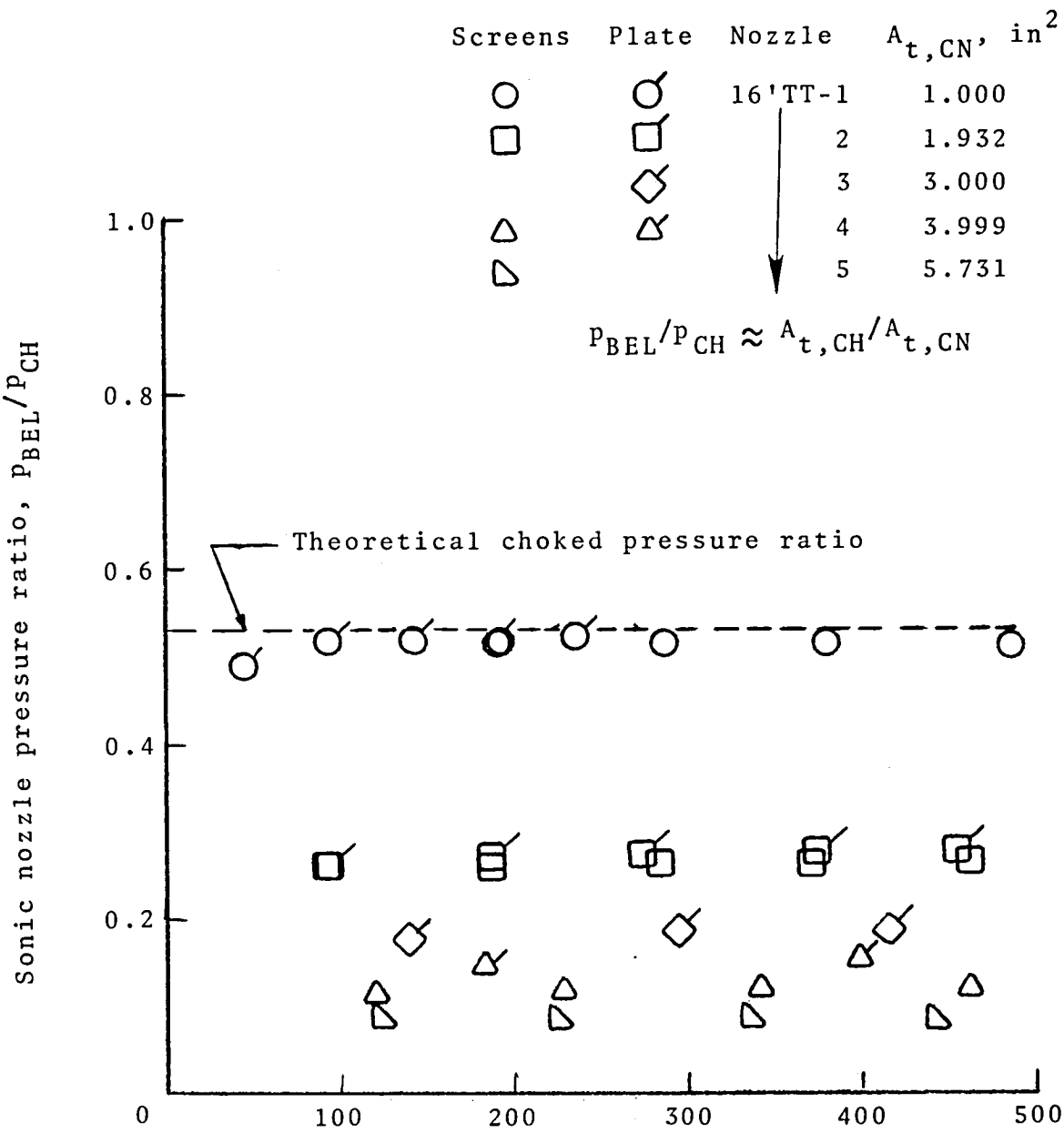

(a) $A_{t,CH,T} = 0.562$ in^2.

Figure 10.- Pressure ratio across sonic nozzles as a function of high-pressure plenum pressure.

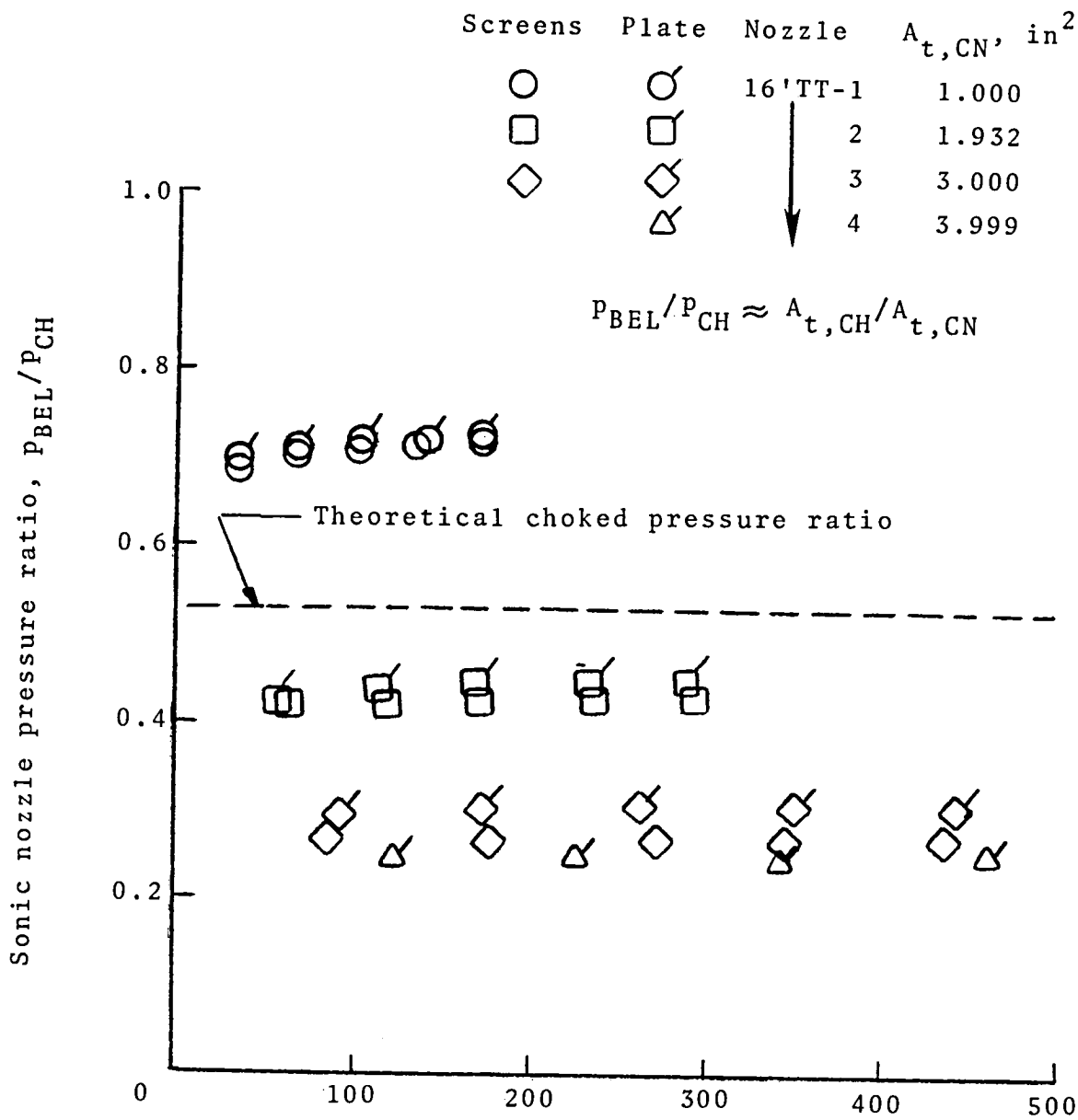

(b) $A_{t,CH,T} = 1.070$ in^2.

Figure 10.- Concluded.

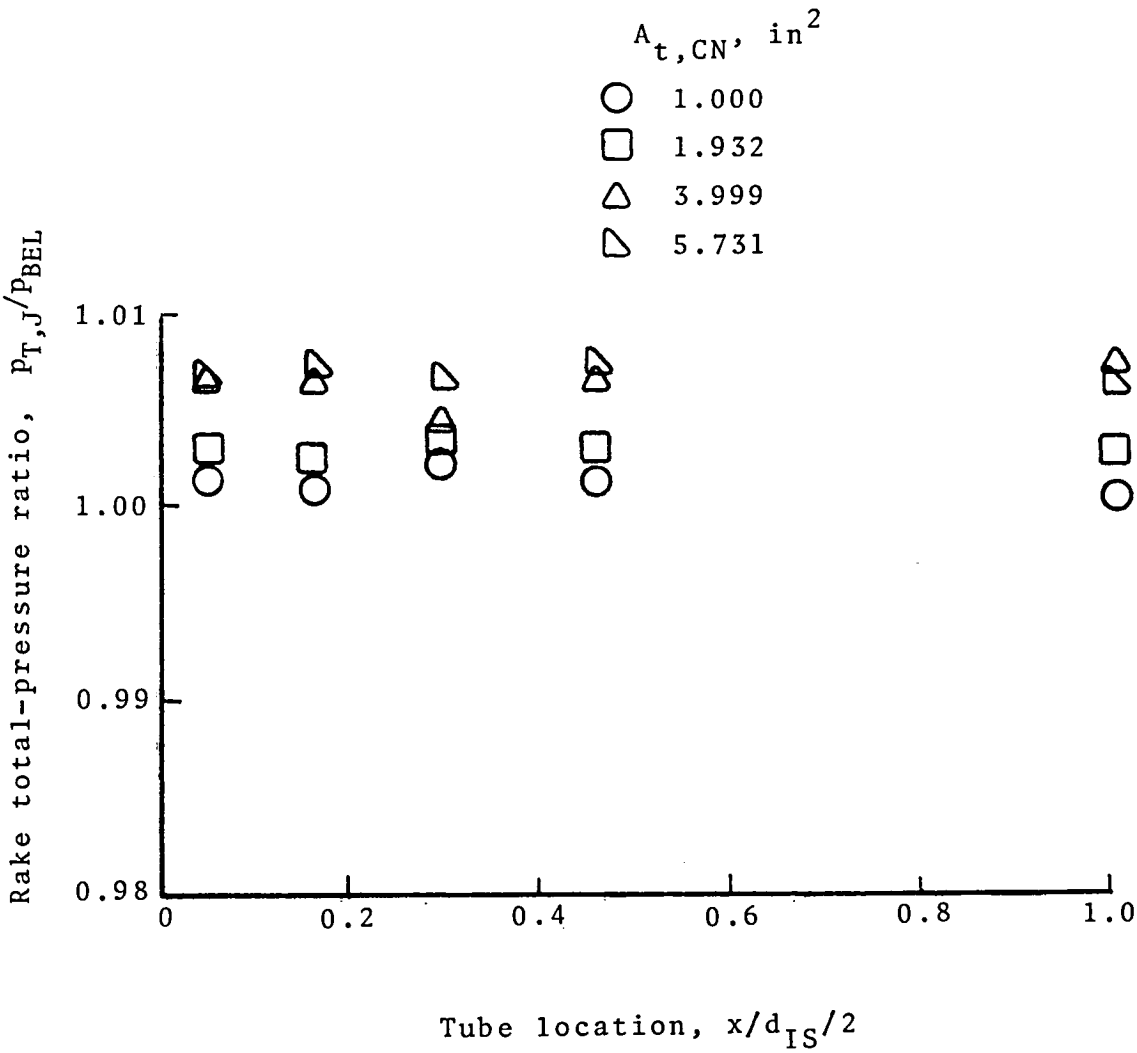

Figure 11.- Typical nozzle total-pressure measurements on rake in instrumentation section with screens.

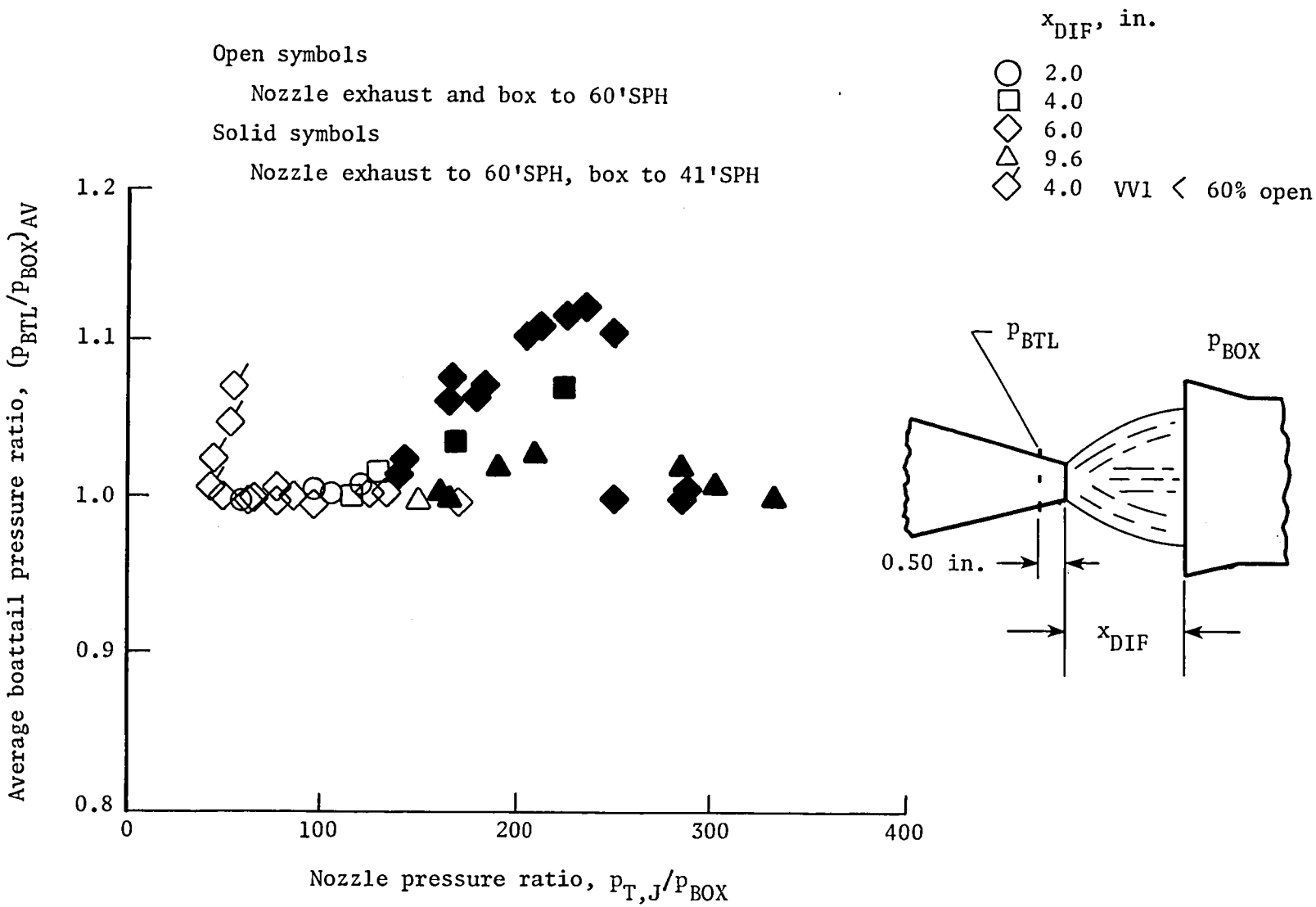

Figure 12.- Nozzle jet interference effects in boattail section of a typical 16'TT calibration nozzle. $A_{t,CN}$ = 1.000 in^2.

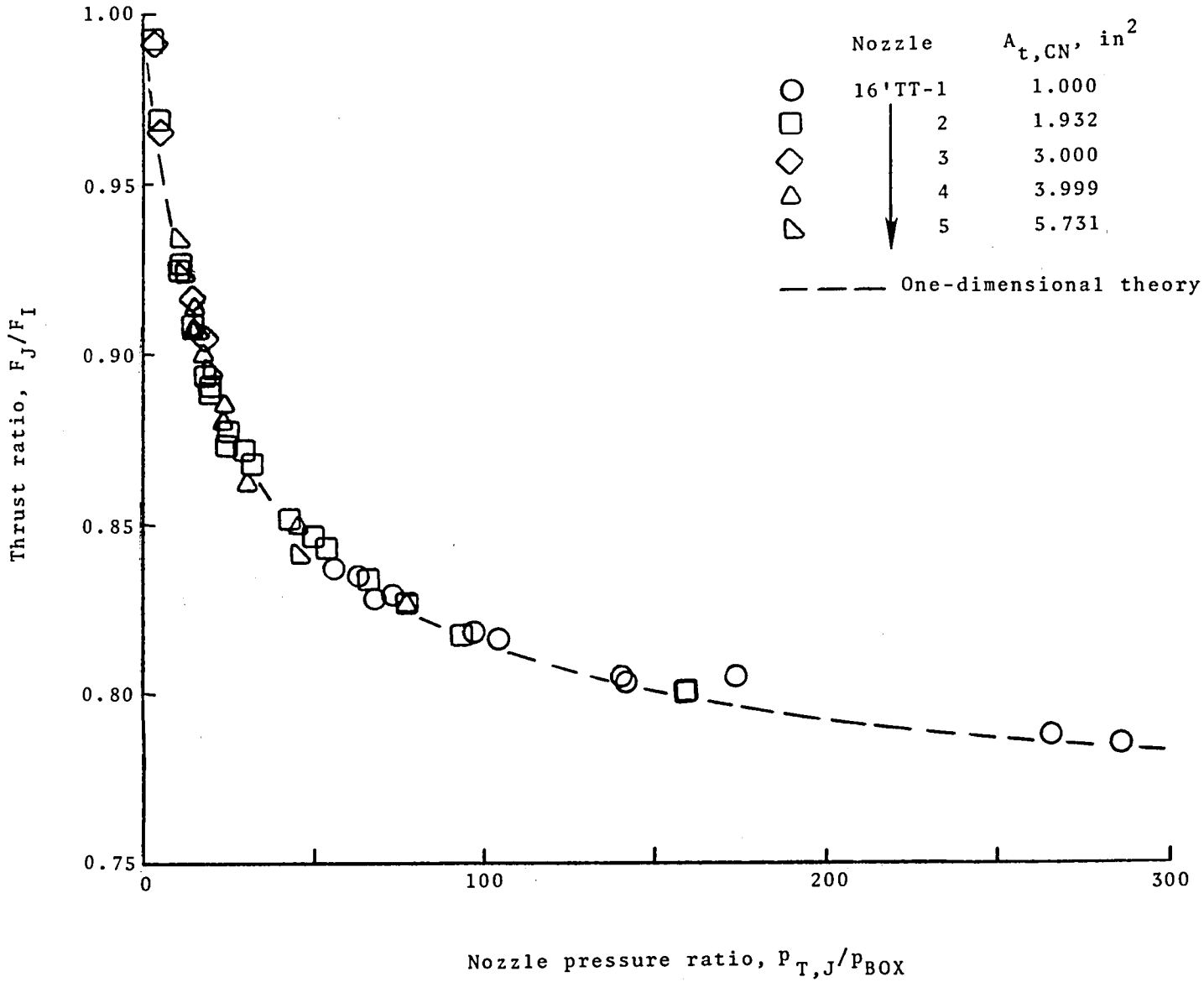

Figure 13.- Static performance of 16'TT calibration nozzles.

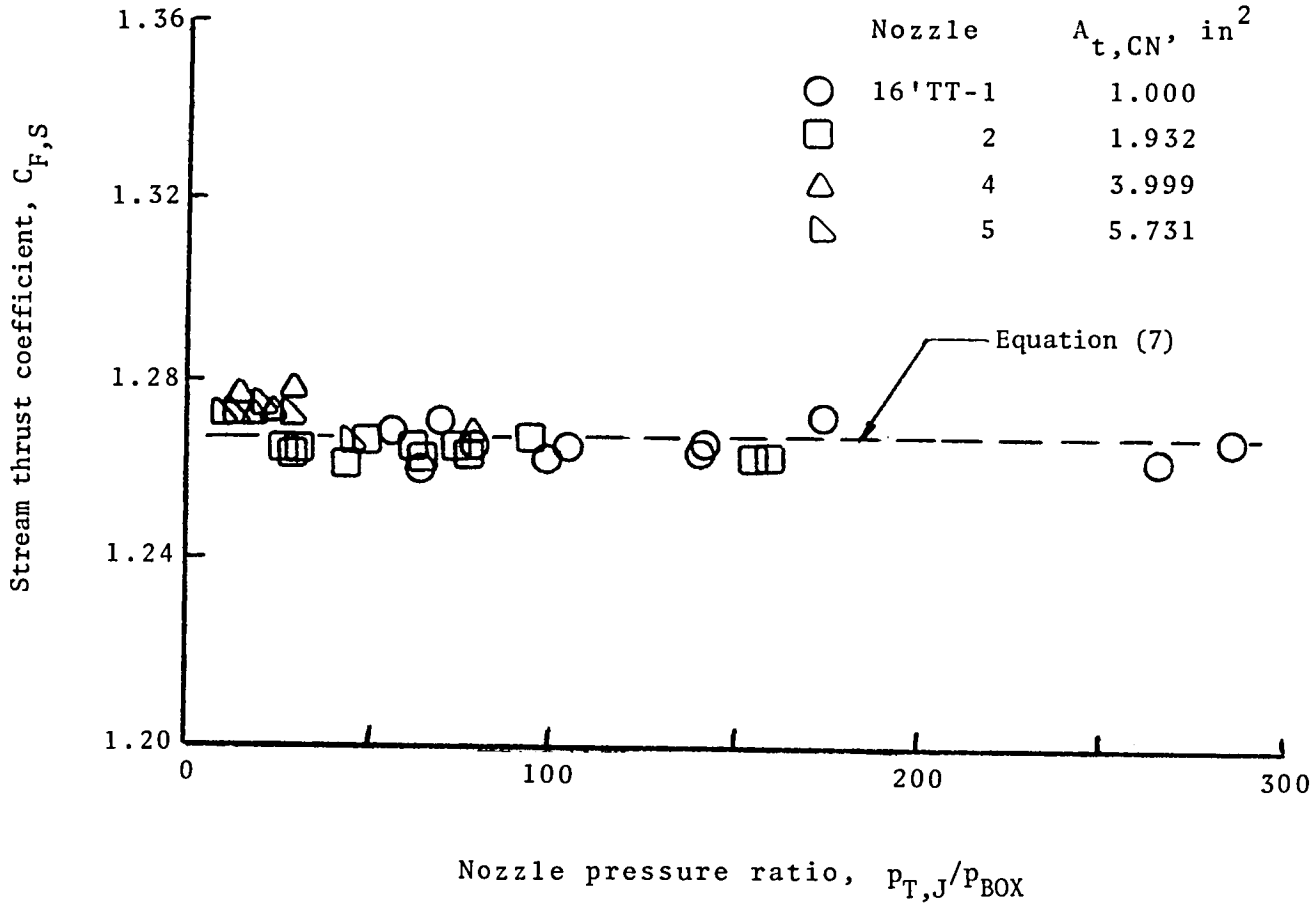

Figure 14.- Variation of stream thrust coefficient with nozzle pressure ratio for 16'TT calibration nozzles.

1. Report No.	2. Government Accession No.	3. Recipient's Catalog No.
NASA TM-86368		

4. Title and Subtitle	5. Report Date
Modifications to the Nozzle Test Chamber To Extend Nozzle Static-Test Capability	May 1985
	6. Performing Organization Code: 505-43-90-03
7. Author(s): J. Wayne Keyes	8. Performing Organization Report No.: L-15674
9. Performing Organization Name and Address: NASA Langley Research Center, Hampton, VA 23665	10. Work Unit No.
	11. Contract or Grant No.
12. Sponsoring Agency Name and Address: National Aeronautics and Space Administration, Washington, DC 20546	13. Type of Report and Period Covered: Technical Memorandum
	14. Sponsoring Agency Code

15. Supplementary Notes

16. Abstract

The nozzle test chamber at the Langley Research Center has been modified to provide a high-pressure-ratio nozzle static-test capability. Experiments were conducted to determine the range of the ratio of nozzle total pressure to chamber pressure and to make direct nozzle thrust measurements using a three-component strain-gage force balance. Pressure ratios from 3 to 285 have been measured with several axisymmetric nozzles at a nozzle total pressure of 15 to 190 psia. Devices for measuring system mass flow were calibrated using standard axisymmetric convergent choked nozzles. System mass-flow rates up to 10 lbm/sec were measured. In general, the measured thrust results of these nozzles were in good agreement with one-dimensional theoretical predictions for convergent nozzles.

17. Key Words (Suggested by Author(s))	18. Distribution Statement
Static-test facility Nozzle performance High nozzle pressure ratios Nozzle flow visualization	Unclassified - Unlimited Subject Category 02

19. Security Classif. (of this report)	20. Security Classif. (of this page)	21. No. of Pages	22. Price
Unclassified	Unclassified	33	A03

N-305 For sale by the National Technical Information Service, Springfield, Virginia 22161 NASA-Langley, 1985